optics

Article

Topological and Optical Properties of Passeriformes' Feathers: Biological UV Reflector Antenna

P. Singh [1], M. A. Jalil [2], P. Yupapin [3], J. Ali [4], M. A. Palomino [5], M. Toledo-Solano [6], K. Misaghian [7,8], J. Faubert [7,8], K. Ray [5,7,9,*], A. Bandyopadhyay [1] and J. E. Lugo [5,7,8,*]

1   Advanced Key Technologies Division, National Institute for Materials Science (NIMS), 1-2-1 Sengen, Tsukuba 305-0047, Japan
2   Department of Physics, Faculty of Science, Universiti Teknologi Malaysia, Skudai 81310, Malaysia
3   Department of Electrical Technology, School of Industrial Technology, Sakonnakhon Technical College, Institute of Vocational Education Northeastern 2, Sakon Nakhon 47000, Thailand
4   Asia Metropolitan University, 6, Jalan Lembah, Bandar Baru Seri Alam, Johor Bahru 81750, Malaysia
5   Facultad de Ciencias Físico-Matematicas, Ciudad Universitaria, Puebla 72570, Mexico
6   Facultad de Ciencias Físico-Matematicas, CONACYT-Benemerita Universidad Autonoma de Puebla, Puebla 72570, Mexico
7   Faubert Lab, Université de Montréal, Montreal, QC H3T 1P1, Canada
8   Sage-Sentinel Smart Solutions, 1919-1 Tancha, Onna-son, Kunigami-gun, Okinawa 904-0495, Japan
9   Department of Physics Amity, School of Applied Sciences, Amity University Rajasthan, Jaipur 303002, India
*   Correspondence: kanadray00@gmail.com (K.R.); eduardo.lugo@sagesentinel.com (J.E.L.)

Abstract: This manuscript explores the topological and optical properties of a Passeriformes bird feather. Inside the feather, the layers of keratin and melanin are responsible for light reflection, transmission, and absorption; notably, the miniature composition of melanosome barbules plays a crucial role in its reflective properties. We adopted a multilayer interference model to investigate light propagation throughout the Passeriformes plume. As a result, we obtained all necessary simulated results, such as resonance band, efficiency, and electromagnetic radiation patterns of the Passeriformes plume, and they were verified with the experimental results reported in the literature study regarding light reflectivity through its internal geometry. Interestingly, we discovered that the interior structure of the Passeriformes plume functions similarly to a UV reflector antenna.

Keywords: Passeriformes; multilayer interference model; UV reflector antenna; resonance frequency

1. Introduction

In the biological world, coloration and geometrical characteristics are vital for demonstrating the optical properties of bird organs [1]. For example, Huth and Burkhardt first detailed birds' tetrachromatic features and UV perceptions of light [2]. Tetrachromatic color vision is found in many birds' eyes, making them capable of perceiving ultraviolet light. On the other hand, it has already been shown that iridescent colors are formed due to the different refractive indexes of different layers (air, keratin, and melanin) in the bird feather. Therefore, visual communication in some birds and animals is achievable by displaying and perceiving iridescent colors. For example, iridescent color is distinguishable in the keratin layer above a single melanin layer of a Passeriformes feather [2]. In earlier studies, the unidirectional and bidirectional geometry of the barbule was described in detail in the barbs' medullar cortex [3–5]. Moreover, one study explored the optical properties of bird feathers in the infrared region of 700–2600nm. In addition, Fox et al. determined the reflectance and transmittance of light in the visible region across the different bird species and examined the variation of light reflection and transmission in the interior morphology of barbules; these parameters vary across other species [6].

Principally, the barbules of the feather are colored by pigment, and selective interference occurs due to light reflection. Such barbules are made from different refractive (low or

high value) index materials. The back-and-forth reflection of light from the barbs generates multiple interference patterns. After that, the keratin/chitin and pigment layers, which are connected physically or chemically, generate the colors [7]. Finally, these colors are produced by the spongy keratin found in medullary cells in the barbule [8]. It is worth mentioning that all the optical properties of barbules depend on the angle of illumination. In that regard, barbules' light reflectivity spectra and directional properties have been measured [9].

An experimental study provided findings to assess the influence of the environment on the development of eumelanic and pheomelanic color in a Passeriformes bird, a black-capped chickadee. The main conclusion was that investigators should exercise caution when attributing variance in melanin-based color to melanin alone, and the microstructure of the feather should be considered [10]. The light reflectance phenomenon reveals unidirectional and three-directional natures of the colored occipital barbules and breast barbules, respectively; these reflection properties are discovered by replicating the realistic structure of the barbules using finite time-domain simulations [11]. Plume morphology is responsible for color formation. The layers inside the barbules manage the phase division in their respective regions [12,13]. However, the morphology of melanosomes varies between iridescent plums of different species [14]. The iridescent color comes from the melanin-containing melanosome, which is organized in an array form [15]. Melanin color is the standard color in the animal world and is significant at the pigmentary stage. The color concentration is illustrated as a substantial deviation in the brightness of the breast plumage [16]. Many studies on plumage coloration examine its role in signaling between animals and their activities. They also illustrate the different coloration systems and their reaction to the incident light [17].

Meticulous studies have been done on how pigment and its internal architecture produce color by light scattering. The geometry of the barbules is the key to absorbing the incident light and producing an enormously low-level light reflection. The super-black plume is a nanostructured morphology of inclined arrays of barbules that create more light scattering than regular black barbules (structural absorption); therefore, super-black plums show extremely low reflection. Barbule morphologies are distinctively different in regular and super black plumes [18,19]. In addition, they have unique mechanical and aerodynamic properties due to their stiffness and lightness. Such properties were studied using speckle pattern interferometry, an optical technique for determining the mechanical activities of the feather and that is capable of determining the optical phase of the nanostructure in the plume [19].

Passeriformes birds are the most abundant bird species on earth, with more than 5000 species. They present beautiful iridescent colors; more than 60% present UV reflection, and 17% reflect UV light with an amplitude between 380 and 399 nm. Moreover, there is evidence that they are capable of having UV vision. Besides the multitudinous amount of Passeriformes birds, more UV-related behavioral studies on these birds are necessary [2].

Signal communication in the biological system has always been discussed [20–22]. However, it is always difficult and expensive for a researcher to experiment with biomaterials at the nano and picoscale. Here, we suggested a reliable simulation method to predict the results regarding the biomaterials. We used our simulated results in simple mathematical calculations to verify our approach's effectiveness and the experimental results reported in the literature study. Furthermore, we can set the experimental parameter conditions according to our simulation findings. In this manuscript, we suggested that the Passeriformes plume behaves as a UV-reflecting antenna when sunlight falls at a certain angle through the elements of the Passeriformes plume.

This work is organized as follows: First, we introduce the methodology to simulate actual results for explaining the optical phenomena regarding the color of a feather. We solved the geometrical pattern of the barbules through the Maxwell equation solver in the time-domain mode. As a result, we found that the topology and material properties of the barbules produce bright colors by light scattering. Interestingly, our simulation

results are analogous to the experimental results found in the literature studies. Second, the simulation and experimental results analysis are discussed in more detail in the Results and Discussion section, and, finally, we obtained our conclusion.

2. Methods

We built the interior geometry of the feather barbules (Figure 1b) by following their original dimensions and material properties (Figure 1a). Using electromagnetic simulation software, we proposed an inner multilayer replica of the barbules of a Passeriformes feather (Figure 1a). We estimated the resonance peaks from the KHz to PHz frequency range. We picked only those peaks that showed a considerable amplitude (Figure 2a, upper left panel). We noted the results regarding resonance peaks, gain, efficiency, and VSWR curves (Figure 2a), which help to explain the experimental literature studies regarding the light mechanism within the barbules. The proposed geometry illustrates the significant peaks in the UV region. We theoretically showed a standard multilayer interference replication to evaluate the feather barbule's reflection spectrum. The built planar multilayer structure consists of top and bottom layers of keratin and melanin; both layers are organized periodically (Figure 2a). The first keratin layer thickness was obtained from [23], and the width of melanin and keratin films was taken from [24], as detailed in Table 1.
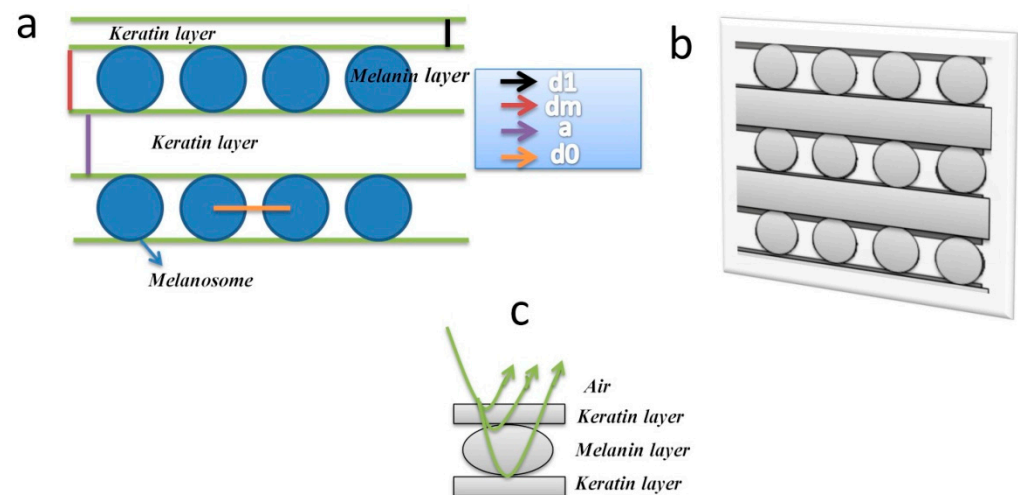
Figure 1. (**a**) Passeriformes feathers' multilayer elements such as the keratin layer, melanin layer, and melanosome; d1, dm, a, and d0 are the symbols of first keratin layer thickness (adapted from [23]), melanin layer thickness, and subsequent keratin layers' thicknesses, which corresponds to melanosomes' diameters, and the distance between melanosome layers [24], respectively. (**b**) A barbules model was created in the electromagnetic simulation software CST (Computer Simulation Technology) to perform the light interaction with barbules [11]. (**c**) A schematic of light reflection through the feather's multiple layers is shown here.

Table 1. The thickness of different layers in the simulated feather [23,24].

Initial Keratin Layer (d1)	Melanosome Diameter (dm)	Keratin Space between Melanosome Layers (a)	Inner-Layer Spacing of Melanosomes (d0)
12 ± 7 nm [23]	200 nm [24]	200 nm [24]	222 nm [24]
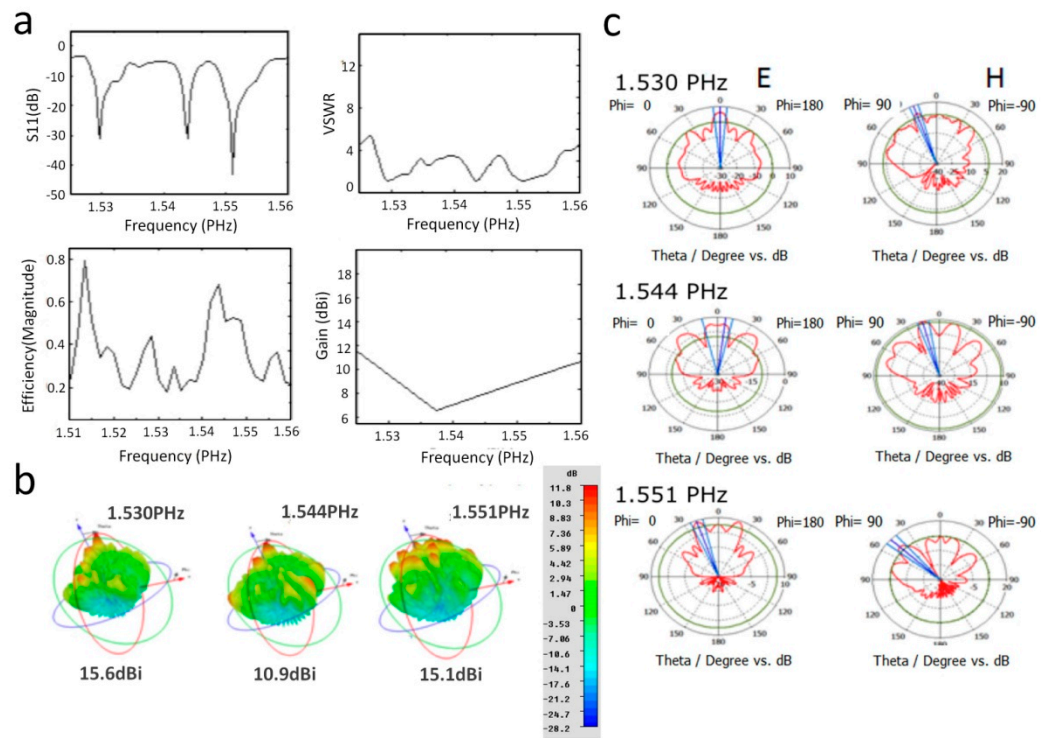
Figure 2. (**a**) Simulated resonance curves (1.525–1.575 PHz) of Passeriformes feather barbule model. The resonance spectrum has three resonance peaks at 1.530 PHz, 1.544 PHz, and 1.551 PHz frequencies. In the right upper panel, the average value of VSWR is almost equal to 1 at all resonance frequencies. High efficiency (65%) is observed at the third resonance peak, 1.544 PHz (bottom, left panel). The created structure in the bottom right panel has a positive gain at resonance peaks. (**b**) Directivity values are 15.6 dBi, 10.9 dBi, and 15.1 dBi at 1.530 PHz, 1.544 PHz, and 1.551 PHz resonance peaks, respectively. (**c**) The variation of E and H radiation patterns at resonance frequencies is shown.

3. Results and Discussion

The optical properties of keratin and melanin layers allow us to evaluate the relative significance these films when light interacts with them (Figure 1c). The keratin layer's refractive index (n_{ker}) as a function of its wavelength is defined as [23,25–27].

$$n_{ker} = 1.532 + \frac{5890}{\lambda^2} \tag{1}$$

where λ is the light wavelength in nm.

The melanin layer absorbs light [28], and it is a combination of keratin and melanosomes. Therefore, the refractive index for this layer is as follows [29]:

$$n_{mel,eff} = n_{eff} - iK_{eff} \tag{2}$$

$$n_{eff}^2 = \frac{\left[A + \sqrt{A^2 + B^2} \right]}{2}$$

$$K_{eff}^2 = \frac{\left[-A + \sqrt{A^2 + B^2} \right]}{2}$$

$$A = f_{mel}(n_{mel}^2 - K_{mel}^2) + (1 - f_{mel})(n_{ker}^2 - K_{ker}^2)$$

$$B = 2f_{mel}n_{mel}K_{mel} + 2(1 - V_{mel})n_{ker}K_{ker}$$

The coefficient f_{mel} is the average melanosome volume fraction in each melanosome layer, and for the dense melanin substance, we have [23]

$$n_{mel} = 1.56 + \frac{36000}{\lambda^2} \tag{3}$$

$$K_{mel} = 1.62e^{\frac{-\lambda}{142}}$$

Using Equations (1)–(3), the values of refractive indexes of keratin and melanin layers at the UV wavelength of 400 nm are 1.57 and 1.71−i0.06, respectively.

Following the simulation antenna analogy, we used the VSWR that measures the load impedance matching to the transmission line characteristic impedance carrying radio frequency (RF) signals. A portion of the forward wave delivered toward the load is reflected down the transmission line toward the source when there is an impedance mismatch between the load and the transmission line. The source then encounters a different impedance than anticipated, which may result in it supplying less power (or more power in certain situations), with the outcome being highly dependent on the length of the transmission line's electrical cable.

Standing waves along the transmission line caused by such a mismatch are typically undesirable and increase transmission line losses (significant at higher frequencies and for longer cables). The VSWR measures the depth of the standing waves, measuring how well the load matches the transmission line. For example, a VSWR of 1:1 would indicate no reflected wave with a matched load. An electrical load with an infinite VSWR reflects all incident power toward the source, since it cannot absorb it.

The equation of the VSWR parameter is given as

$$VSWR = \frac{1 + |\Gamma|}{1 - |\Gamma|} \tag{4}$$

where Γ represents the reflection coefficient.

3.1. Light Propagation from Air to Keratin Layer

When the light propagates from the air medium ($n_{air} = 1$) to the keratin (n_{ker}) = 1.57 medium (Figure 1c) through the normal of the incidence plane, then the equations for the reflection coefficients will be as follows [30]:

$$\Gamma = \frac{n_{air}\cos(\theta_k) - n_{ker}\cos(\theta_l)}{n_{air}\cos(\theta_k) + n_{ker}\cos(\theta_l)} \tag{5}$$

where θ_k and θ_l are the incidence and transmitted angle, respectively, for TE polarization, and θ_k and θ_l are the transmitted and incidence angle, respectively, for TM polarization.

Now, placing Equation (5) in Equation (4) to find the VSWR for both polarizations is carried out as follows:

$$VSWR = \frac{n_{air}\cos(\theta_k)}{n_{ker}\cos(\theta_l)} \tag{6}$$

Furthermore, we used Snell's law to obtain the transmitted angle as a function of the incidence angle.

The VSWR obtained from the simulation was close to one at the resonance peaks, as shown in Figure 2a, right top panel. As seen in Figure 3 (top), at the resonance, there was no reflection for TM polarization light at an angle close to 57°. This angle corresponds to Brewster's condition given by $\theta_{Brewster} = Tan^{-1}(n_{ker}/n_{air}) = 57.5°$. Both curves correlate with the reflectivity, calculated as $|\Gamma|^2$ (see Figure 3b. Then, when the electric field is perpendicular to the air–keratin interface, the reflectivity amplitude should increase with the angle of incidence (TE polarization).
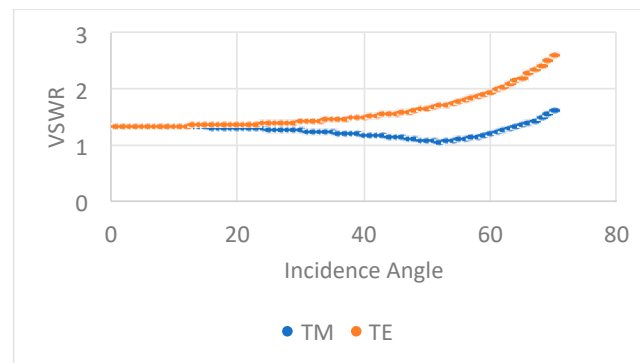
(a)

(b)
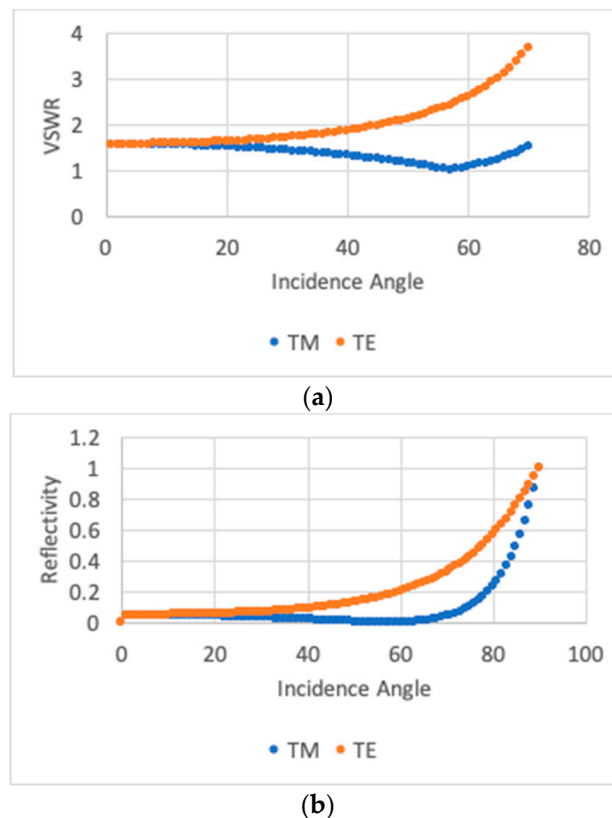
Figure 3. (**a**) VSWR for TE and TM polarizations in the UV region at the air–keratin interface. VSWR, which is measured from one to five, is higher than one for all incidence angles in the case of TE polarization. At the resonance frequency, the VSWR is close to one, corresponding to Brewster's angle condition or equivalently zero reflectivity for TM polarization. (**b**). Reflectivity spectrum for TE and TM polarizations in the UV region at the air–keratin interface. We can observe that both graphs displayed correlate with each other.

On the contrary, the TM reflectivity amplitude should decrease for angles of incidence less than Brewster's angle and increase again up to 90^0. Our results are consistent with experimental results in the bird-of-paradise (Lawes' parotia) and the Japanese Jewel Beetle (*Chrysochroa fulgidissima*). An earlier study showed that in Lawes' parotia, the reflectance amplitude of TE-polarized light or electric vector monotonically increased with the angle θ_i, whereas the reflectivity amplitude of TM-polarized light or magnetic vector decreased in the range of θ_i from angles of 55° to 60°, although beyond a 60° angle, the reflectivity amplitude increased linearly with θi. Similarly, in *Chrysochroa fulgidissima,* for TE-polarized light, the peak reflectance increased with an increasing angle of incidence for both the green and purple areas, but for TM-polarized light, the peak reflectance decreased, becoming minimal at an angle of incidence of ~65–70°; at larger angles, the overall spectral reflectance increased again [11,25].

3.2. Light Propagation from the Keratin Layer to the Melanin Layer

As the light wave propagates from keratin to melanin(see Figure 1c), the VSWR is close to one for angles below Brewster's angle ($\theta_{Brewster} = Tan^{-1}(Re(n_{mel)}/n_{ker})) = 47.4°$ for both polarizations (Figure 4). Under such conditions, the reflectivity is very low. Consequently, within an angular region beyond Brewster's angle, UV-light interference mostly happens in Passeriformes' feathers. However, it is known that melanin is not a lossless material and absorbs light within the NIR–VIS–UV range [11,24,25,28]. Therefore, to better understand the reflectivity behavior, we calculated the reflectivity from 250 nm up to 25 microns using the transfer matrix method [31].

Figure 4. VSWR for TE and TM polarizations in the UV region at the keratin–melanin interface; VSWR is higher than one for all incidence angles. From our simulation results, VSWR values go from one to five. At resonance, the VSWR is close to one, corresponding to Brewster's angle condition or equivalently zero reflectivity for TM polarization.

3.3. Multilayer Analysis

A multilayer interference reflector is based on the refractive index and thickness of the layers, assuming that the melanin layers are not lossless (from Section 3.2). The relation between the maximum reflectivity wavelength, thicknesses, and refractive indexes is given by [25,32,33]:

$$\lambda_1 = 2(n_{\text{ker}}dl + n_{mel}dm) \tag{7}$$

Its harmonics is given by:

$$\lambda_i = \frac{\lambda_1}{i} \quad i = 2, 3, 4 \dots$$

Again, $n_{\text{ker}} = 1.57$ and $\text{Re}(n_{mel}) = 1.71$, and $dl = 200$ nm are used as the thickness of the keratin layer, while $dm = 200$ nm is used as the thickness of the melanin layer (Figure 1a) (Table 1); these values are placed in Equation (6) to obtain:

$$\lambda_1 = 1311 \text{ nm} \tag{8}$$

$$\lambda_2 = 655 \text{ nm}$$

$$\lambda_3 = 436 \text{ nm}$$

$$\lambda_4 = 328 \text{ nm}$$

$$\lambda_5 = 262 \text{ nm}$$

According to this, there may be two bands with high reflectivity in the near-infrared and visible red regions, and three or more high reflectivity bands in the violet–ultraviolet region. Please bear in mind that these bands' locations are approximated because Equation (7) holds for lossless materials only, but it is a good approximation. However, the absorption effects are introduced using the transfer matrix method [31], where the refractive indexes can be complex, and their imaginary part reflects the material's absorption. Therefore, the values of refractive indexes of keratin and melanin layers used here were calculated using Equations (1) and (3) with values of 1.57 and 1.71-i0.06, respectively.

In Figure 5, four reflectivity bands are observed (red lines). We used the normalized frequency given by $\omega = 2\pi(dl + dm)/\lambda$, which is dimensionless. One band belongs to the infrared region with a peak at 1237 nm, another in the violet region at 437 nm, and two ultraviolet bands at 333 nm and 284 nm. The reflectivity calculation holds for both TE and TM polarizations because the angle of incidence is zero. There is no reflectivity band within the red region. The trade-off between light absorption and reflection may cause this. The real part of the refractive index value of melanin is not high enough to overcome its imaginary part value, and consequently, absorption beats reflection, killing

any constructive interference. A Passeriformes feather's average reflectivity spectrum was measured [10] in the region from 300 to 700 nm. The average reflectivity was $6.4 \pm 0.39\%$. An average of $6.7 \pm 2.3\%$ was calculated from the theoretical spectrum at an angle of incidence $0°$. Accordingly, with the above reflectivity analysis, if we increase the incidence angle, the reflectivity should increase at any angle for TE polarization. We calculated the reflectivity spectrum under this condition (Figure 6), and the average reflectivity increased up to $21.1 \pm 4.5\%$ when the angle of incidence was $57°$. In addition, three bands shifted towards the UV region, contributing to a higher UV light reflectivity.
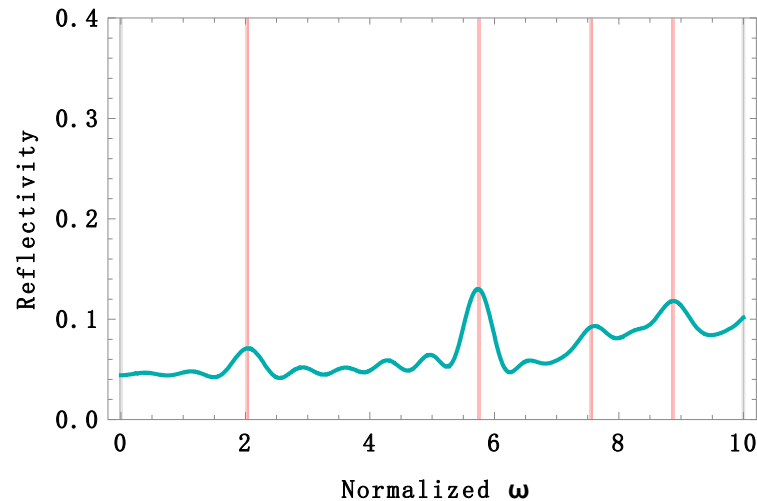
Figure 5. Theoretical reflectivity spectrum of the simulated barbule feather for TE, TM polarization, and incidence angle of $0°$. Four high reflectivity bands (red lines) can be observed at 1237 nm, 437 nm, 333 nm, and 284 nm. The average reflectivity from 300 to 700 nm was $6.7 \pm 2.3\%$, close to the experimental value of $6.4 \pm 0.39\%$ measured in [10]. A UV-chroma of 27% was calculated in the same range, and a UV-chroma of $24 \pm 0.19\%$ was reported in [10]. The normalized frequency is given by $\omega = 2\pi(dl + dm)/\lambda$.
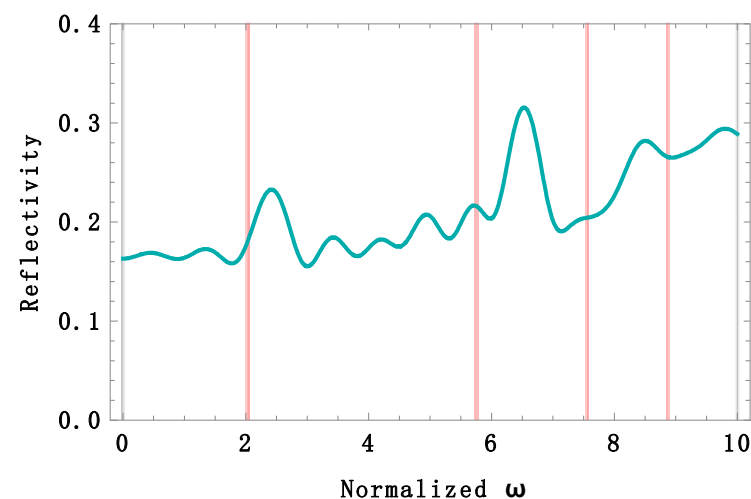
Figure 6. Theoretical reflectivity spectrum of the simulated feather for TE polarization and incidence angle of $57°$. Four high reflectivity bands shifted towards the UV region. The red lines at 1237 nm, 437 nm, 333 nm, and 284 nm represented the positions of the peaks when the angle of incidence was $0°$. The average reflectivity from 300 to 700 nm increased up to $21.1 \pm 4.5\%$. A UV-chroma of 30% was calculated in the same range. The normalized frequency is given by $\omega = 2\pi(dl + dm)/\lambda$.

The UV-chroma is an important parameter to measure UV light contributions to reflectivity. It is measured as the proportion of total reflectivity occurring within 300–400 nm. For

example, a UV-chroma of 24 ± 0.19% was reported in [10]. We calculated the UV-chroma from our two spectra and found values of 27% ($\theta_i = 0°$) and 30% ($\theta_i = 57°$).

3.4. UV Antenna

The radiated pattern of the feather shown in Figure 2c is similar to the power radiated in parabolic antennas. Therefore, for simplicity, we could treat the barbule of the feather as an array of parabolic antennas, each antenna having a directivity or diversity *D* given by [34].

$$D = \frac{4\pi(Area)}{\lambda^2} \tag{9}$$

furthermore, the directivity is related to the gain *G* as:

$$G = eD \tag{10}$$

where *e* is the antenna's efficiency.

In practice, the efficiency value of the parabolic antenna lies in the 50–65% range [34], which is well suited to our simulated efficiency (Figure 2a, bottom left panel).

The area of a melanosome is given by $4\pi d_m^2/4$, and using the wavelength at the three resonance peaks (195.9 nm, 194.2 nm, and 193.3 nm); the theoretical directivities given by Equation (9) are 16.14 dBi, 16.21 dBi, and 16.25 dBi, respectively, and these values coincide with the order of magnitude of our simulated results, which are revealed in Figure 2b (bottom right panel).

4. Conclusions

Here we have suggested a narrative approach to match the literature results by the simulation techniques regarding the light interaction mechanisms in the internal geometry of barbule feathers of Passeriformes birds. Simulations have been performed to detect the reflection coefficient (S11), efficiency, VSWR, gain, directivity, and radiation pattern. We have concluded based on the topological and optical properties of the Passeriformes feather barbules. As discussed in the above sections, the barbules of the Passeriformes bird feather act as a UV reflector antenna. There is good similarity between our simulation findings and the experimental results of literature studies. Simulation results confirm that the intended approach is effective.

Specifically, our simulation and theoretical results are accurate enough compared to earlier findings. For instance, the theoretical reflectivity spectrum intensity of the simulated barbule feather for TE, TM polarization, and incidence angle of 0° was 10%. This result is akin to FDT modeling of a similar feather, as shown in [11], or multilayer modeling with a gradient refractive index [24]. Moreover, for TE polarization, our calculated reflectivity spectrum intensity in the UV band was 20–32% when the angle of incidence was 57°. In [11], in the FDT simulation under TE polarization and angles of incidence between 50° and 60°, the reflectivity spectrum intensity was 20–27%. Moreover, we found the average reflectivity from 300 to 700 nm was 6.7 ± 2.3%, close to the experimental value of 6.4 ± 0.39% measured in [10]. A UV-chroma of 27% was calculated in the same range, and a UV-chroma of 24 ± 0.19% was reported in [10].

Finally, the feather barbules have resonance peaks in the PHz frequency range, and their layers play an important role in displaying iridescent colors. We demonstrated conditions of maximum or minimum light reflection in layers of a Passeriformes feather with varying incident light angles. The property that barbules behave as a UV reflector antenna could help in the design of new solar cell applications.

Author Contributions: Conceptualization, P.S., K.R., A.B. and J.E.L.; methodology, P.S., K.R., A.B. and J.E.L.; software, J.F. and K.R.; validation, P.S., K.M., A.B. and J.E.L.; formal analysis, P.S., K.R. and J.E.L.; investigation, P.S. and J.E.L.; resources, P.S., M.A.J., P.Y., J.A., M.A.P., M.T.-S., K.M., J.F., K.R., A.B. and J.E.L.; data curation, P.S.; writing—original draft preparation, P.S., K.R., A.B. and J.E.L.; writing—review and editing, P.S., M.A.J., P.Y., J.A., M.A.P., M.T.-S., K.M., J.F., K.R., A.B. and J.E.L.;

References

1. Yoshioka, S.; Kinoshita, S. Effect of Macroscopic Structure in Iridescent Color of the Peacock Feathers. *Forma* **2002**, *17*, 169–181.
2. Mullen, P.; Pohland, G. Studies on UV reflection in feathers of some 1000 bird Species: Are UV peaks in feathers correlated with violet-sensitive and ultraviolet-sensitive cones. *J. Compil.* **2008**, *150*, 59–68. [CrossRef]
3. Greenwalt, C.H.; Brandt, W.; Friel, D.D. Iridescent colors of hummingbird feathers. *J. Opt. Soc. Am.* **1960**, *50*, 1005–1013. [CrossRef]
4. Prum, R.O.; Torres, R.; Williamson, S.; Dyck, J. Constructive inference of light by blue feather barbs. *Nature* **1998**, *396*, 28–29. [CrossRef]
5. Shawkey, M.D.; Saranathan, V.; Pa'lsdo'ttir, H.; Crum, J.; Ellisman, M.H.; Auer, M.; Prum, R.O. Electron tomography, three-dimensional Fourier analysis and color prediction of a three-dimensional amorphous biophotonic nanostructure. *J. R. Soc. Interface* **2009**, *6*, S213–S220. [CrossRef]
6. Stuart-Fox, D.; Newton, E.; Mulder, R.A.; D'Alba, L.; Shawkey, M.D.; Igic, B. The microstructure of white feathers predicts their visible and near-infrared reflectance properties. *PLoS ONE* **2018**, *13*, e0199129. [CrossRef]
7. Shawkey, M.D.; Morehouse, N.I.; Vukusic, P. A protean palette: Color materials and mixing in birds and butterflies. *J. R. Soc. Interface* **2009**, *6*, S221–S231. [CrossRef]
8. Saranathan, V.; Forster, J.D.; Noh, H.; Liew, S.-F.; Mochrie Simon, G.J.; Cao, H.; Dufresne Eric, R.; Prum Richard, O. Structure and optical function of amorphous photonic nanostructures from avian feather barbs: A comparative small-angle X-ray scattering (SAXS) analysis of 230 bird species. *J. R. Soc. Interface* **2012**, *9*, 2563–2580. [CrossRef]
9. Osorio, D.; Ham, A.D. Spectral reflectance and directional properties of structural coloration in bird plumage. *J. Exp. Biol.* **2002**, *205*, 2017–2027. [CrossRef]
10. D'Alba, L.; Van Hemert, C.; Spencer, K.A.; Heidinger, B.J.; Gill, L.; Evans, N.P.; Monaghan, P.; Handel, C.M.; Shawkey, M.D. Melanin-Based Color of Plumage: Role of Condition and of Feathers' Microstructure. *Integr. Comp. Biol.* **2014**, *54*, 633–644. [CrossRef]
11. Wiltsa, B.D.; Michielsenb, K.; Raedta, H.D.; Stavenga, D.G. Sparkling feather reflections of a bird-of-paradise are explained by finite-difference time-domain modeling. *Proc. Natl. Acad. Sci. USA* **2014**, *111*, 4363–4368. [CrossRef] [PubMed]
12. Parnell, A.J.; Washington, A.L.; Mykhaylyk, O.O.; Hill, C.J.; Bianco, A.; Burg, S.L.; Dennison, A.J.; Snape, M.; Cadby, A.J.; Smith, A.; et al. Spatially modulated structural colour in bird feathers. *Sci. Rep.* **2015**, *5*, 18317. [CrossRef] [PubMed]
13. Stavenga, D.G. Thin film and multilayer optics cause structural colors of many insects and birds. *Mater. Today Proc.* **2014**, *1*, 109–121. [CrossRef]
14. Norden, K.K.; Faber, J.W.; Babarović, F.; Stubbs, T.L.; Selly, T.; Schiffbauer, J.D.; Štefanić, P.P.; Mayr, G.; Smithwick, F.M.; Vinther, J. Melanosome diversity and convergence in the evolution of iridescent avian feathers—Implications for paleocolor reconstruction. *Evolution* **2019**, *73*, 15–27. [CrossRef]
15. Eliason, C.M.; Bitton, P.P.; Shawkey, M.D. How hollow melanosomes affect iridescent colour production in birds. *Proc. R. Soc. B Biol. Sci.* **2013**, *280*, 1505. [CrossRef]
16. Mcgraw, K.J.; Safran, R.J.; Wakamatsu, K. How feather color reflects its melanin content. *Funct. Ecol.* **2005**, *19*, 816–821. [CrossRef]
17. Riedler, R.; Pesme, C.; Druzik, J.; Gleeson, M. A review of color-producing mechanisms in feathers and their influence on preventive conservation strategies. *J. Am. Inst. Conserv.* **2014**, *53*, 44–65. [CrossRef]
18. McCoy, D.E.; Feo, T.; Harvey, T.A.; Prum, R.O. Structural absorption by barbule microstructures of super black bird of paradise feathers. *Nat. Commun.* **2018**, *9*, 1–8. [CrossRef]
19. Torre-Ibarra, M.H.; Santoy, F.M.M. Interferometric study on bird's feather. *J. Biomed. Opt.* **2013**, *18*, 056011. [CrossRef]
20. Singh, P.; Doti, R.; Lugo, J.E.; Faubert, J.; Rawat, S.; Ghosh, S.; Bandyopadhyay, A. Biological Infrared Antenna and Radar. In *Soft Computing: Theories and Applications*; Advances in Intelligent Systems and, Computing; Pant, M., Ray, K., Sharma, T., Rawat, S., Bandyopadhyay, A., Eds.; Springer: Singapore, 2018; Volume 584, pp. 223–232.
21. Singh, P.; Doti, R.; Lugo, J.E.; Faubert, J.; Rawat, S.; Ghosh, S.; Bandyopadhyay, A. DNA as an Electromagnetic Fractal Cavity Resonator: Its Universal Sensing and Fractal Antenna Behavior. In *Soft Computing: Theories and Applications*; Advances in Intelligent Systems and Computing; Pant, M., Ray, K., Sharma, T., Rawat, S., Bandyopadhyay, A., Eds.; Springer: Singapore, 2018; Volume 584, pp. 213–223.

22. Singh, P.; Doti, R.; Lugo, J.E.; Faubert, J.; Rawat, S.; Ghosh, S.; Bandyopadhyay, A. Fractal and Periodical Biological Antennas: Hidden Topologies in DNA, Wasps and Retina in the Eye. In *Soft Computing Applications*; Studies in Computational Intelligence; Ray, K., Pant, M., Bandyopadhyay, A., Eds.; Springer: Singapore, 2018; Volume 761, pp. 113–123.

23. Xiao, M.; Dhinojwala, A.; Shawkey, M. Nanostructural basis of rainbow-like iridescence in common bronzewing Phaps chalcoptera feathers. *Opt. Express* **2014**, *22*, 14627. [CrossRef]

24. Stavenga, D.G.; Leertouwer, H.L.; Osorio, D.C.; Wilts, B.D. High refractive index of melanin in shiny occipital feathers of a bird of paradise. *Light Sci. Appl.* **2015**, *4*, 1–6. [CrossRef]

25. Wilts, B.D. Brilliant Biophotonics: Physical Properties, Pigmentary Tuning & Biological Implications. Ph.D. Thesis, University of Groningen, Groningen, The Netherlands, 2013.

26. Leertouwer, H.L.; Wilts, B.D.; Stavenga, D.G. Refractive index and dispersion of butterfly chitin and bird keratin measured by polarizing interference microscopy. *Opt. Express* **2011**, *19*, 24061–24066. [CrossRef] [PubMed]

27. Yoshioka, S.; Kinoshita, S. Direct determination of the refractive index of natural multilayer systems. *Phys. Rev. E Stat. Nonlin. Soft Matter Phys.* **2011**, *83*, 051917. [CrossRef] [PubMed]

28. Wolbarsht, M.L.; Walsh, A.W.; George, G. Melanin, a unique biological absorber. *Appl. Opt.* **1981**, *20*, 2184–2186. [CrossRef]

29. Sihvola, A.H. *Electromagnetic Mixing Formulas and Applications*; The Institution of Engineering and Technology: Herts, UK, 1999.

30. Alexander, I.L. Fresnel Equations. 2013. Available online: https://docslib.org/doc/6183407/fresnel-equations-alexander-i (accessed on 12 February 2022).

31. Sambit, S.; Abhishek, P.; Chittaranjan, N. Transfer matrix optimization of a one- dimensional photonic crystal cavity for enhanced absorption of monolayer graphene. *Appl. Opt.* **2022**, *61*, 8613–8623.

32. Kinoshita, S. *Structural Colors in the Realm of Nature*; World Scientific: Singapore, 2008.

33. Land, M.F. The physics and biology of animal reflectors. *Progr. Biophys.* **1972**, *24*, 77–105. [CrossRef]

34. Sandeep, K.M.; Sumi, K. A Review Paper on Microwave Transmission using Reflector Antennas. *Int. J. Sci. Eng. Res.* **2017**, *8*, 251–254.